Journal of Applied Sciences and Nanotechnology

Journal homepage: https://jasn.uotechnology.edu.iq/

Enhancing Gas Sensing Performance through Laser Ablation Characterization of Silver@Gold Bimetallic Nanoparticles

[1]Yasemin H. Khadim*, [1]Uday M. Nayef, [2]Falah A-H. Mutlak

[1]Department of Applied Sciences, University of Technology – Iraq

[2]Department of Physics, College of Science, University of Baghdad – Iraq

Article information

Article history:
Received: October, 12, 2023
Accepted: January, 23, 2024
Available online: March, 10, 2024

Keywords:
Silver@ Gold,
Gas senser,
Porous silicon,
Laser ablation

Corresponding Author:
Yasemin H. Khadim
as.21.48@grad.uotechnology.edu.iq

Abstract

This investigation analyzes the impact of a laser pulse energy set at 700 millijoules per pulse on silver, gold, and silver@gold nanoparticles deposited onto porous silicon (PS). Our primary objective is to discern optimal conditions by comprehensively evaluating their influence on structural, electrical, morphological, and optical characteristics. Employing pulsed laser ablation in liquid, an Nd:YAG laser featuring a 10-nanosecond pulse width and a 1064 nm wavelength is utilized for nanoparticle creation. X-ray diffraction analysis (XRD) is employed to affirm the crystalline growth of core-shell nanoparticles, with distinct peaks in the data confirming the presence of both Au and Ag nanoparticles. Morphological analysis reveals a robust attachment between the nanoparticles and the porous silicon layer, indicating structural stability. The UV–vis spectra exhibit a localized surface plasmon resonance (LSPR) band within the 412–521 nm range. Notably, with an increase in gold concentration, the two peaks of the LSPR band converge into a singular peak. Comparison of the photoluminescence emission spectra of the PS substrate and NPs/PS demonstrates a significant broadening of the emission band in PS, indicative of high-quality porous silicon structure. The intriguing characteristics of Ag@Au NPs make them promising for application in gas sensor systems.

DOI: 10.53293/jasn.2023.7137.1252, Department of Applied Sciences, University of Technology - Iraq.

1. Introduction

It is possible to tailor NPs with exceptional optical, electrical, mechanical, and magnetic properties [1-2]. These NPs are useful in human-centric fields due to their unique properties and different plasmonic, electrical, and highly catalytic activities. They provide adaptability across various industries. By varying their morphology, structure, size, and surface properties, Au, Ag, and Ag@ Au nanostructures with different compositions can have different properties [3-4]. Top-down methods are increasingly being used to create bimetallic colloids [5]. A pure silver plate placed in 1 ml of hexadecyltrimethylammonium bromide (CTAB) and 4 ml of redistilled deionized water was exposed to laser radiation. The purity of resultant products and monodispersity is greatly depend on the concentration of the CTAB solution. To produce high-quality and adjustable Au NPs, it is therefore crucial to

choose the right CTAB concentrations [6–7]. The precise focus of the 1064 nm pulsed laser was at a beam angle of 90° incidence. Each pulse had a duration of 10 ns and a pulse energy of 700 mJ. There were 100 repetitions of each pulse. The Ag plate was then replaced with an Au plate inside the glass cell to produce Ag@ Au NPs. The core particle size and/or shell thickness of core-shell NPs can be changed, based primarily on the incident laser energy concentrated on the material [8]. It is possible to modify the final sizes and optical characteristics of the nanoparticles [9-10]. The PLAL technique produces high-purity nanomaterials that stand out for their simplicity, affordability, speed, and environmental friendliness [11–12]. The PLAL method can be used to create almost any kind of nanoparticle [13–14]. Since NPs can be made from any solid material, laser ablation is a tried-and-true, safe method for producing pure nanomaterials [15]. Wet-chemical techniques can yield a wide range of forms and compositions of colloidal nanoparticles, but they have limitations due to contaminations and residual reactions that severely limit their applications. Because of its remarkable properties, an optical material that can be tailored through electrochemical silicon etching is a nanomaterial that is highly desirable for a number of applications. PS techniques are used in many semiconductor devices [16–17]. Ag@ Au nanoparticles were deposited onto PS to increase the NPs' ability to detect toxic gases (H2S and NO2) as a function of operating temperature. Ag and Au NPs were also compared [18-19]. In this work, we used the PLAL ablation technique to create NP materials, which we then deposited on PS substrates. Using XRD, PL, and SEM analyses, the produced Ag, Au, and Ag@Au NPs were evaluated for surface morphology, optical characteristics, and crystallinity. Additionally, the electrical and sensitivity characteristics of the device were evaluated at a laser pulse energy of 700 mJ.

2. Experimental Procedures

Cetrimonium bromide (CTAB) and distilled water were mixed to create nanoparticles using the PLAL technique, as shown in Fig. 1. An Nd: YAG laser operating at a wavelength of 1064 nm and with a pulse duration of 9 ns was used. CTAB powder (Mw: 364.45 g/mol) comes from Scientific Polymer Products, Inc., located in New York, state of America. The pure silver metal plate was first subjected to 100 laser pulses at 700 millijoules of laser energy while submerged in a mixture of CTAB and distilled water. There was a silver nanofluid created. Subsequently, the pure gold plate was substituted for the silver plate in the nanofluid and subjected to an identical sequence of pulses and laser energy, resulting in the formation of a silver@gold core-shell nano colloidal. The laser used had a wavelength of 1064 nm. The silicon was then electrochemically etched from a monocrystalline n-type silicon substrate and placed onto a PS substrate. PS films were created using silicon wafers of a (111) orientation with sheet resistance varying from 1 to 10 Ω.cm. The etching process took 15 s, and the current density employed to create the films was 25 mA/cm^2. As seen in Fig. 1, the yield nanoparticles were deposited on the PS.

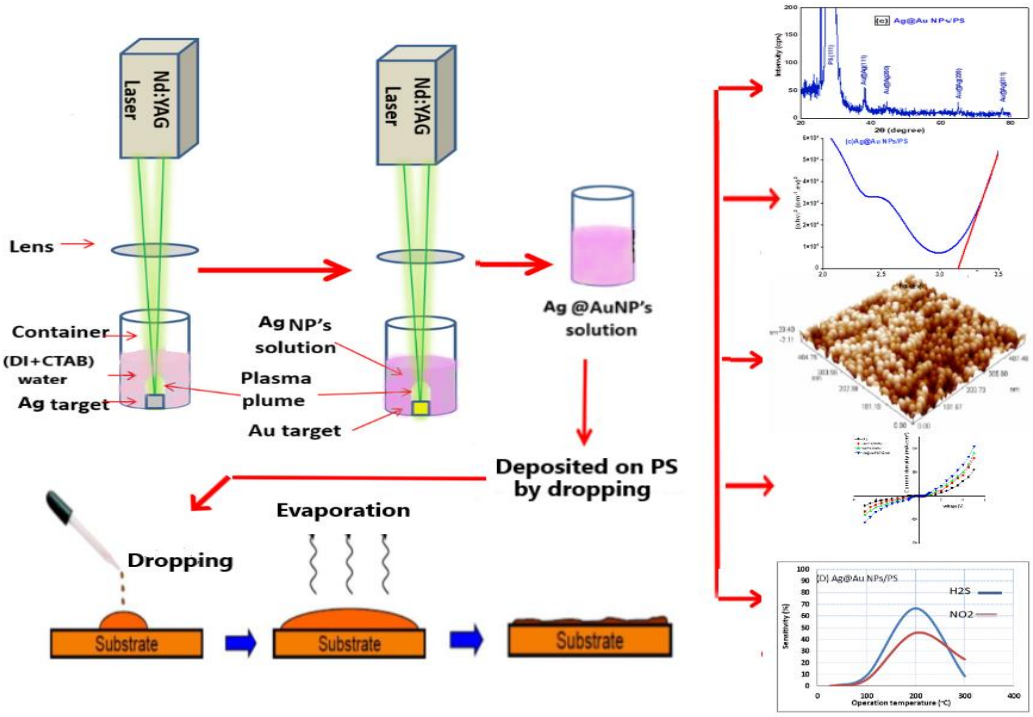

Figure 1: The PLAL technique and the deposition the nanoparticles on the PS.

X-ray diffractometer was used to perform diffraction measurements. A fluorescence spectrophotometer was used to produce photoluminescence emission spectra. UV–vis spectrophotometer was used to record the colloidal solutions optical absorption spectra. A power supply with applied voltage ranging from 0 to 5 V in forward and reverse bias was used to measure the J-V characteristics of Ag, Au, and Ag@Au deposits in the porous silicon structure under Jph-V illumination and dark circumstances.

3. Results and discussion

Fig. 2 shows the XRD patterns of the NPs/PS specimens that were obtained via laser ablation at an energy of 700 mJ and deposited on PS substrates. The significant peak at 29.300 oriented (111) shows broadening across the full width at half maximum (FWHM) due to the nanoscale size of the porous silicon layers. The Ag@ Au NPs' diffraction peaks correspond to the standard JCPDS data cards [3]. The formation of cubic crystal of Ag@ Au core-shell NPs is indicated by the peak values for diffraction at 2Θ = 44.60, 2Θ = 64.70, and 2Θ = 77.60, which correspond to the (111), (200), (220), and (311) planes, respectively.

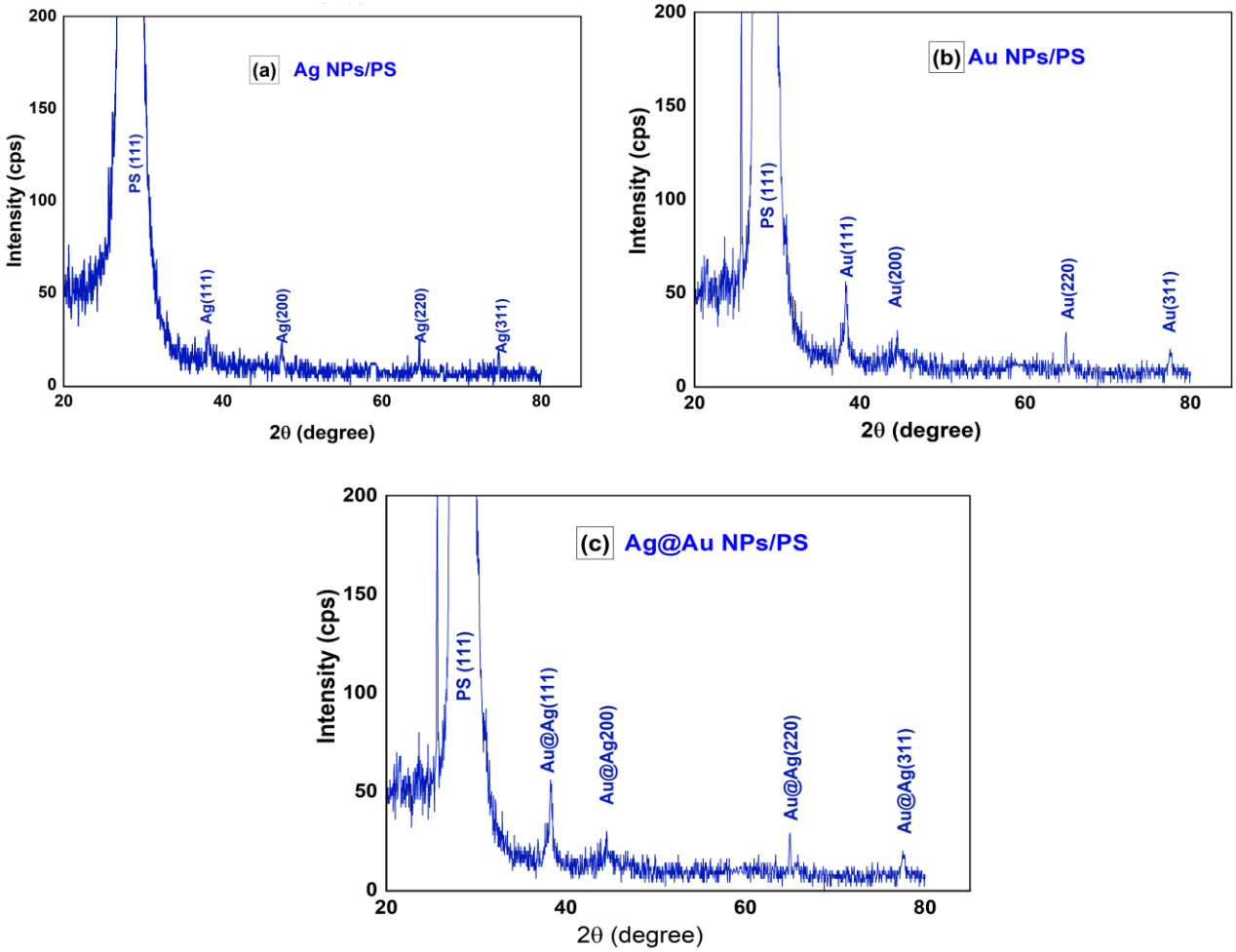

Figure 2: XRD patterns of (a) Ag, (b) Au, and (c) Ag@ Au nanoparticles.

Fig. 3 illustrates the AFM images of the porous silicon structure obtained with 25 mA/cm^2 etching current density and silver@gold core-shell NPs synthesized by laser ablation at 700mJ per pulse deposited on PS substrate. According to Fig. 3A surface morphology, some pores resemble sponges and have an average diameter of 25.80 nm.The prepared Ag@Au NPs' surface morphology or roughness is what makes them that way. Ag@Au NPs had an average roughness that was higher than PS's (see Fig. 3B). The fragmentation of nanoparticles is blamed for this. Ag@Au NP colloids were abundant in the pores, as evidenced by the AFM image, which showed spherical Ag@Au NPs with an average diameter of 23.34 nm and an average roughness of 5.65 nm. Moreover, the image displays a non-uniform distribution of nanoparticles in various sizes, shapes, and heights.

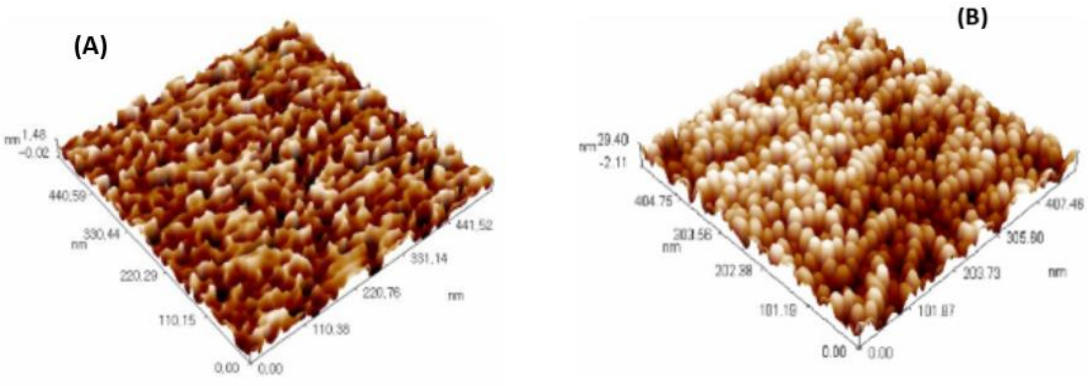

Figure 3: AFM images of (A) porous silicon, and (B) silver@gold core-shell NPs.

The spectra representation of absorption for the solutions of nanoparticles generated by laser ablation at 700 mJ per pulse is shown in Fig. 4. The wavelength scans used for this measurement ranged from 250 to 900 nanometers. The absorption characteristics of the silver nanoparticle solution are demonstrated in Fig. 4A, which shows a semi-symmetric absorption band with a centre wavelength of 412 nm. Similarly, the absorption peak of the gold nanoparticles in Fig. 4B is located at 521 nm. This result is in line with the findings in reference [15]; suggests that most of the nanoparticles in the solution have a spherical form. If gold and silver nanoparticles were mixed in the same solution, the anticipated outcome would be the appearance of two distinct plasmon bands, as shown in Fig. 4C. In particular, wavelengths between 412 and 521 nm are frequently where the peak maxima can be found. It's crucial to observe the noticeable increase in absorbance when contrasting bimetallic nanoparticles with their single nanoparticle counterparts.

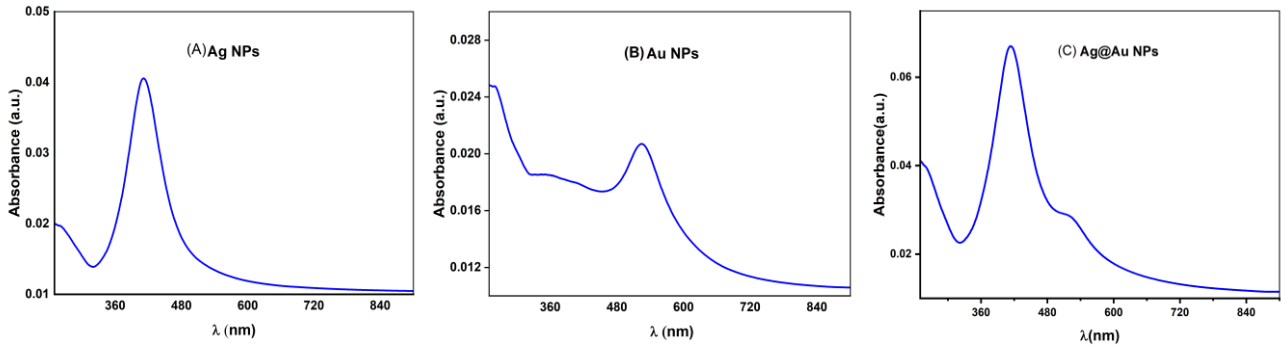

Figure 4: Absorption spectra of (A) Ag, (B) Au, and (C) Ag@Au core-shell NPs.

This behavior can be attributed to the combination's higher concentration of nanoparticles. The appearance of a single-surface plasmon peak indicates that the formed nanoparticles are spherical. Fig. 5 show the energy gaps of the synthesized colloids were calculated by plotting $\alpha h\nu$ vs. photon energy ($h\nu$). The point at which a tangent drawn at the Tauc plot's inflection point intersects the horizontal axis (eV value) yields the band gap value. Eg values are obtained from calculating the energy gaps of NPs: Ag (Eg = 2.55 eV), Au (Eg = 2.35 eV), and Ag@ Au (Eg = 3.15 eV). This phenomenon has a quantum-confined interpretation in which the absorption edge shifts towards shorter wavelengths with decreasing particle size.

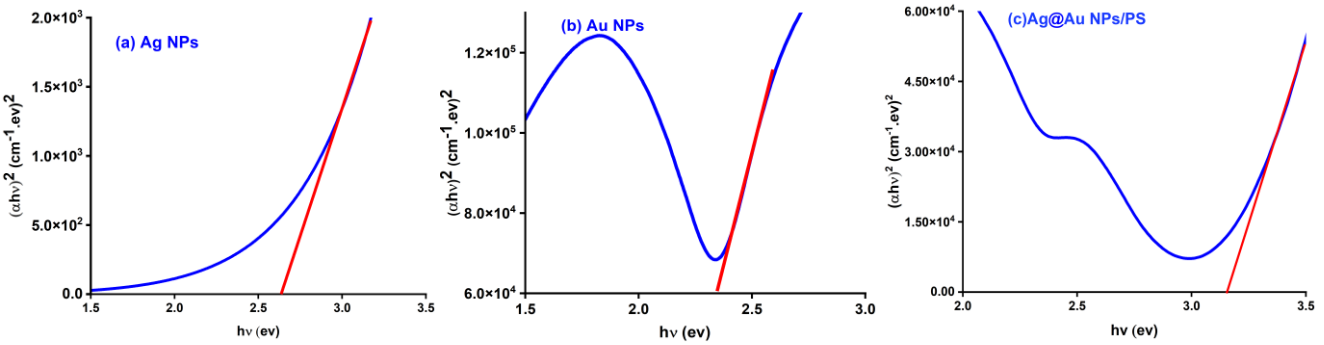

Figure 5: Energy gap of (a) Ag, (b) Au, and (c) Ag@Au NPs synthezied with 700mJ laser pulse energy.

Fig. 6 a shows the PS sample's photoluminescence spectrum at room temperature. The fundamental absorption of porous silicon is represented by an observable peak that arises at 625 nm, with a corresponding energy gap of Eg = 2.01 eV. Silver nanoparticles photoluminescence spectra in Fig. 6 b, show a single peak at 558 nm, which corresponds to an energy gap of 2.22 eV. Likewise, gold exhibits a peak at 570 nm in Fig. 6 c, which corresponds to an Eg = 2.3 eV. On the other hand, a bimetal structure appears in the silver@gold case. At (530 and 630) nm, which correspond to Eg = (2.36 and 2.04 eV), Fig. 6 d, displays two distinct and broad peaks. The observed outcomes differ from the projected amounts of optical absorption, which could be accounted for by the occurrence of trapping states in both gold and silver band gaps.

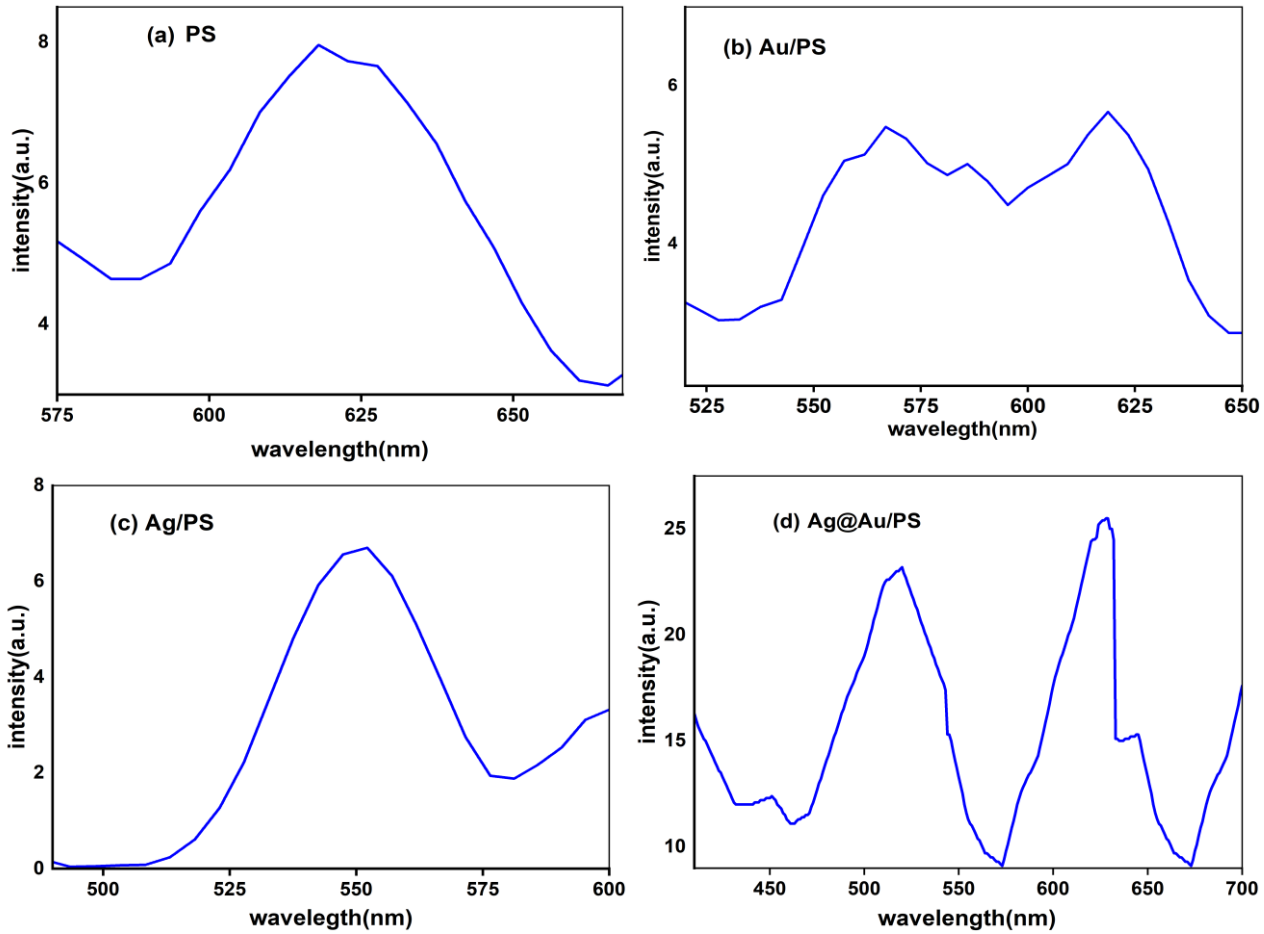

Figure 6: PL spectra of (a) PS with 25mA/cm^2 current density at etching time 15 min. (b) Au, (c) Ag, and (d) Ag@ Au nanoparticles prepared with 700mJ energy.

The J-V characteristic responses for porous silicon, silver, gold, and silver@gold colloid nanoparticle formations under forward and reverse biases are displayed in Fig. 7. In particular, the PS exhibits the behaviour of a perfect diode due to its incredibly small reverse current density. Furthermore, a consistent recombination current is observed at a fairly constant range of forward currents (0.6 Volte). Above a forward current of 0.6 Volte, a noticeable increase in current is evident, which results from the applied voltage surpassing the potential barrier. A featured region where the generated current is dominant forms in the reverse bias, and the current increases with the applied voltage. For the nanoparticle samples with (V > 1 Volte), the lower resistivity of the PS layer results in an increase in forward current, which is followed by a decrease in leakage current at low bias voltages (<1 Volte).

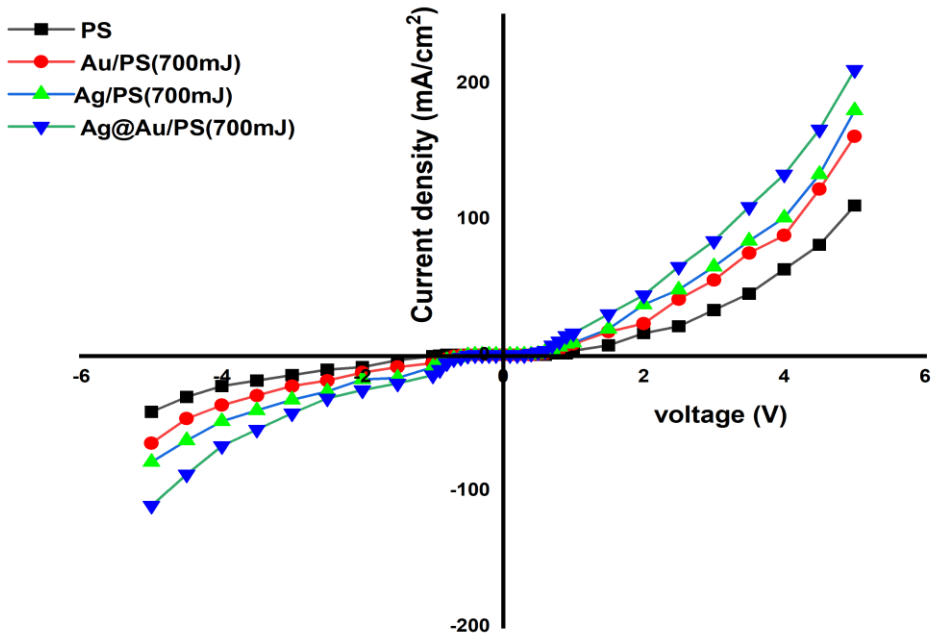

Figure 7: The dark J-V properties of porous silicon, silver, gold, and silver@gold nanoparticles.

The Ag@Au NPs sample, followed by the silver and gold arrangements, has a higher current density than the other samples, according to the J-V curves. Down below 1 V, the forward current is still quite low. At low V values, a phenomenon known as recombination current arises from each electron moving from the valence band into the conduction band. In the second bending zone, the results are dependent on series resistance at high bias voltages. Because of the bias voltage, electrons in this domain have access to sufficient energy. On the other hand, there is a region where the reverse current under the reverse bias increases as the applied voltage increases, creating a discernible current.

The Jph-V characteristics for porous silicon and nanoparticles placed on PS under illumination are illustrated in Fig. 8. Increasing the applied power may result in higher output currents, as more photogenerated carriers are produced. Generally, as the bandwidth gap increases, the resulting currents decrease for the same amount of light power supplied. One of the main causes of the notable increase in photocurrent density at high incident power is the Ag@Au /PS structure's extremely high conductivity. It is worth noting that the reverse current density is greater in the case of bimetallic compared to monometallic nanoparticles.

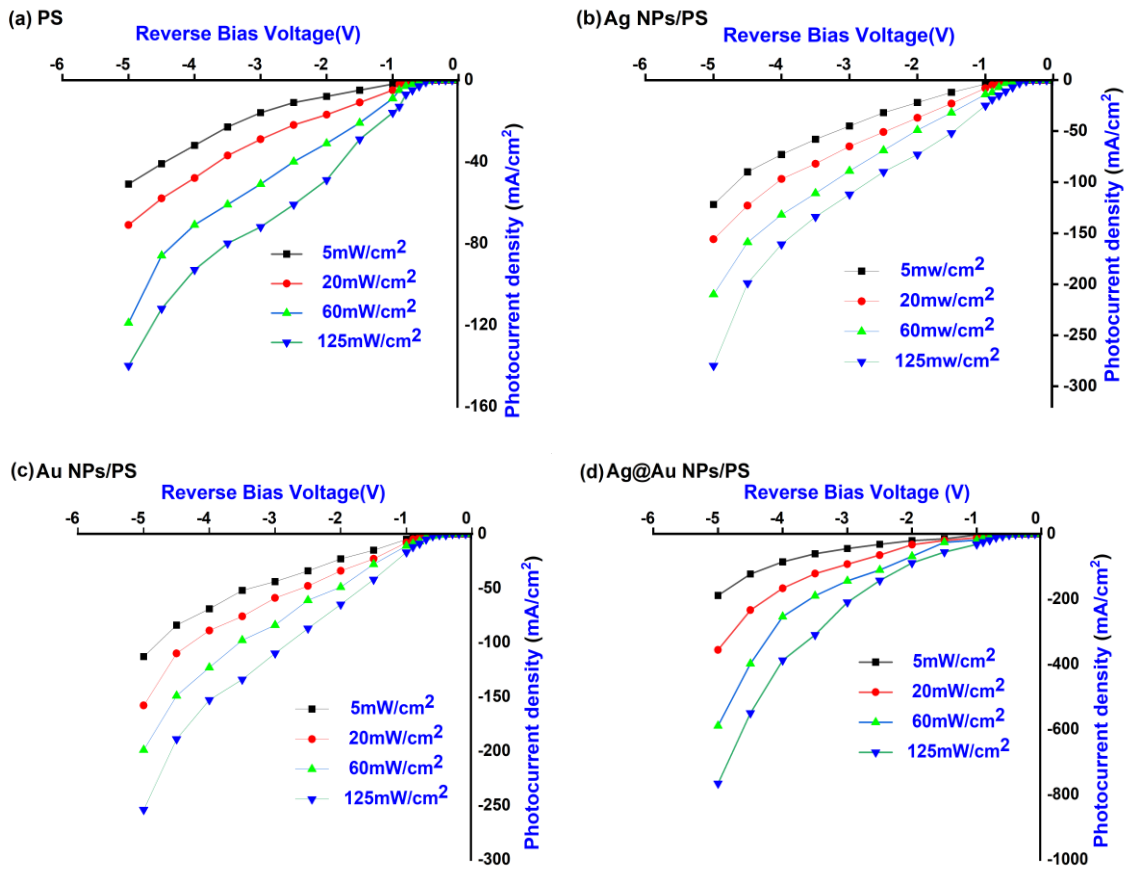

Figure 8: The J_{phto}-V behavior for (a) PS, (b) Ag, (c) Au, and (d) Ag@Au NPs.

Fig. 9, shows the laser ablation technique's ability to construct a silver, gold, and silver@gold NPs/PS gas sensor with high sensitivity to detect H_2S and NO_2 gases. The findings demonstrate that the development of PS increases the thin film's surface area, hence improving its sensitivity to the NO_2 and H_2S gases [18]. The ideal number of surface imperfections, higher porosity, and increased surface area are responsible for this improved sensitivity. Response time is the amount of time that takes for a sensor to change to 19.8% of its initial measurement once the gas flow is interrupted. In the porous silicon, recovery time is used to denote the amount of time required to restore 90% of the initial baseline. The response time examined for silver was equal to 19.2, gold =24.5, and silver@gold =23. The recovery time for H_2S gas was 54% for silver, 99% for gold, and 61% for silver@gold. The response and recovery times, on the other hand, were quicker when dealing with NO_2 gas, demonstrating decreased sensitivity to this gas. The relationship between these reactions and recovery times and changes in operating temperature is seen in Fig. 10.

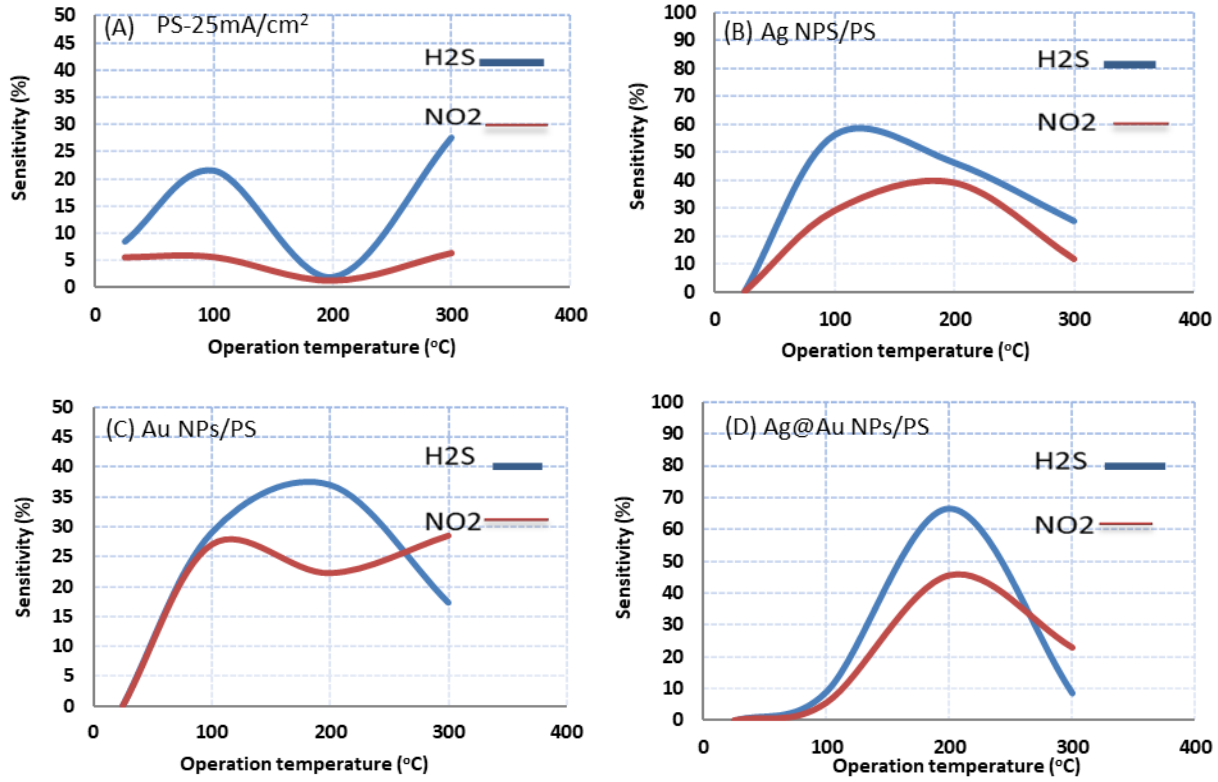

Figure 9: The sensitivity for (A) PS, (B) Ag, (C) Au, and (D) Ag@Au nanoparticles.

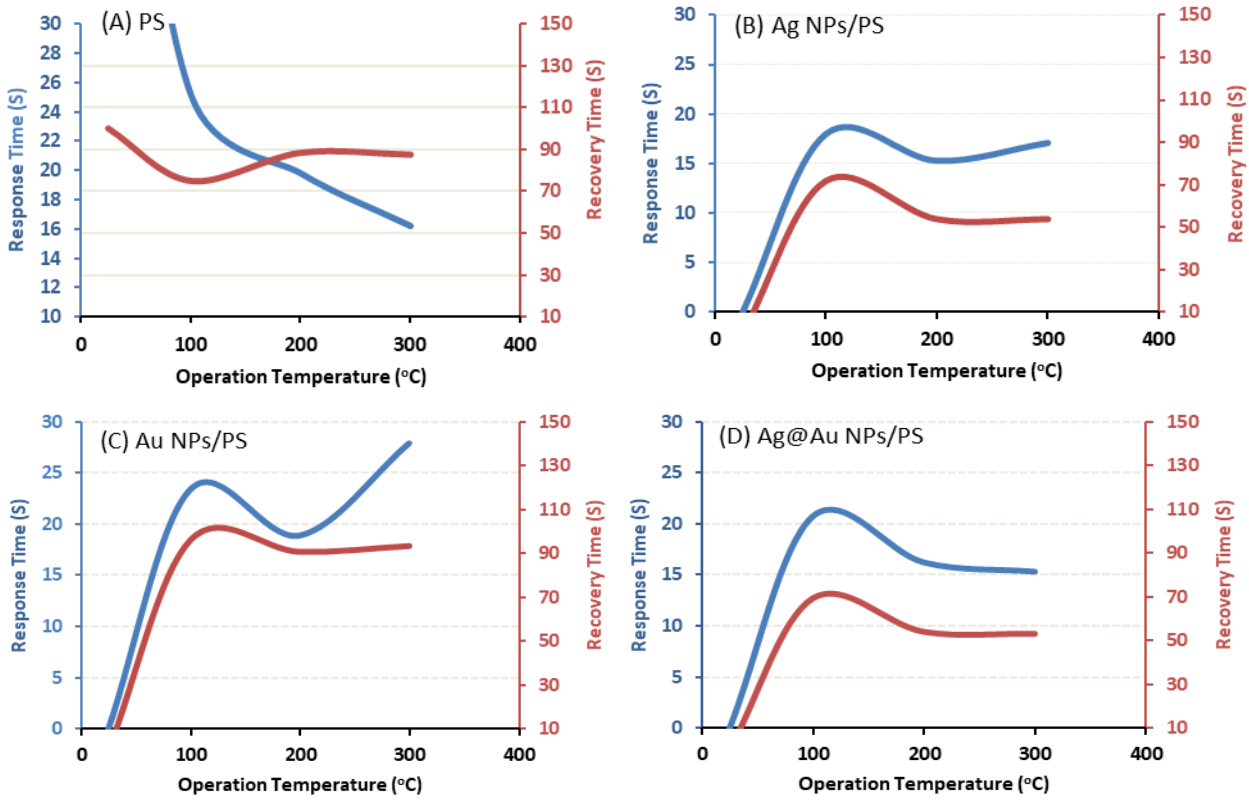

Figure 10: Time of response and recovery of (A) PS, (B) Ag, (C) Au, and (D) Ag@Au NPs towards H_2S gas.

4. Conclusions

Photo-electrochemical etching and pulsed laser ablation have proven to be very helpful techniques for producing silver and gold monometallic NPs as well as silver@gold bimetallic NPs. These techniques are also very affordable and accurate. By varying the applied current density, PS samples' structural properties and light emission can be changed in the context of optoelectronic and sensing device applications. Bimetallic nanoparticles outperformed their monometallic counterparts in terms of performance, indicating an improvement. The electro-optical properties of the devices are improved by using NPs as opposed to PS. It has been shown that the Ag, Au, and Ag@Au nanoparticles contribute more to the improvement of gas sensitivity than the PS layer.

Acknowledgements

The authors would like to thank the University of Technology-Iraq for the logistic support of this work.

Conflict of Interest

The authors declare that they have no conflict of interest.

References

[1] U. M. Nayef and M.W. Muayad, "Typical of Morphological Properties of Porous Silicon," *International Journal of Basic & Applied Sciences*, vol.13, p.15-17, 2013.

[2] M. A. Abed, F.A. Mutlak, A.F. Ahmed, U. M. Nayef, S.K. Abdulridha, and M.S. Jabir, "Synthesis of Ag/Au (core/shell) nanoparticles by laser ablation in liquid and study of their toxicity on blood human components,". J Phys: Conf Series, vol. 1795, p. 012013, 2021.

[3] V. Amendola and M. Meneghetti, "What controls the composition and the structure of nanomaterials generated by laser ablation in liquid solution," Physical Chemistry Chemical Physics, vol. 15, p. 3027–3046, 2013.

[4] F. A. Mutlak, A.F. Ahmed, U.M. Nayef, Q. Al-zaidi, and S.K. Abdulridha, "Improvement of absorption light of laser texturing on silicon surface for optoelectronic application," *Optik*, vol. 237, p.166755, 2021

[5] R. A.Hikmet and N.N.Hussein, "The Biological Activity of Mycosynthesized Silver Nanoparticles against Some Pathogenic Bacteria," *Journal of Applied Sciences and Nanotechnology*, vol. 2, p. 59–68, 2022.

[6] S. Eustis and M.A. El-Sayed," Why Gold Nanoparticles are More Precious Than Pretty Gold: Noble Metal Surface Plasmon Resonance and its Enhancement of The Radiative and Nonradiative Properties of Nanocrystals of Different Shapes," *Chemical society reviews*, vol.35, p.209–217, 2006.

[7] G. Compagnini, E. Messina, O. Puglisi, R. S. Cataliotti, and V. Nicolosi, "Spectroscopic evidence of a core–shell structure in the earlier formation stages of Au–Ag nanoparticles by pulsed laser ablation in water," *Chemical Physics Letters*, vol. 457, p.386–390, 2008.

[8] H. K. Abood and F.A. Mutlak, "Structural, morphological and optical properties of n-type porous silicon-effect of etching current density," *Materials Science and Engineering*: Conference Series, vol. 757, p. 012065, 2020.

[9] H. M. Fadhil, H. A. Salih, and K. I. Hassoon, "Spectroscopic and Structural Analysis of Aluminum Bulk and Nanoparticles: A Comparative Study," *Journal of Applied Sciences and Nanotechnology*, vol. 2, p. 85-94 2022.

[10] U.M. Nayef, K.A. Hubeatir, and Z.J. Abdulkareem, "Characterisation of TiO_2 nanoparticles on porous silicon for optoelectronics application," *Materials Technology*, vol. 31, p.884-889, 2016.

[11] F. A. Mutlak, M. Jaber, and H. Emad, "Effect of laser pulse energy on the characteristics of Au nanoparticles and applications in medicine," *Iraqi journal of science*, vol.58, p.2364–2369, 2017.

[12] A. F. Ahmed, M. R. Abdulameer, M.M. Kadhim, and, F.A. Mutlak, "Plasma parameters of Au nano-particles ablated on porous silicon produced via Nd-YAG laser at 355 nm for sensing NH3 gas," *Optik*, vol. 249, p.168260, 2022.

[13] D. H. Jwied, U.M. Nayef, and F.A. Mutlak, "Synthesis of C: Se (core:shell) nanoparticles via laser ablation on porous silicon for photodetector application," *Optik*, vol.231, p.166493, 2002.

[14] J. Neddersen, G. Chumanov, and T. M. Cotton, "Laser ablation of metals: a new method for preparing SERS active colloids," *Applied Spectroscopy*, vol. 47, p. 1959–1964, 1993.

[15] H. Han, Y. Fang, Z. Li, and H. Xu, "Tunable Surface Plasma Resonance Frequency in Ag Core/Au Shell Nanoparticles System Prepared by Laser Ablation," *Applied Physics Letters*, vol. 92, p.023116, 2008.

[16] M. A. Abed, F. A. Mutlak, M. S. Jabir, and A. F. Ahmed, "Toxicity analysis of Ag/Au core/shell nanoparticles synthesizes via seed-growth on blood human components," *AIP Conference Proceedings*, vol.2372, p.100004, 2021.

[17] U. M. Nayef, I. M. Khudhair, and E. Kayahan, "Organic vapor sensor using photoluminescence of laser ablated gold nanoparticles on porous silicon," *Optik*, vol.144, p.546–552, 2017.
[18] N. S. Dawood, M. Q. Zayer, and M. F. Jawad, "Preparation and Characteristics Study of Porous Silicon for Vacuum Sensor Application," *Karbala International Journal of Modern Science*, vol. 8, p. 105–113, 2022.
[19] M.S. Shore, J. Wang, A. C. Johnston-Peck, A. L. Oldenburg, and J. B. Tracy, "Synthesis of Au (Core)/Ag (Shell) nanoparticles and their conversion to Au: Ag alloy nanoparticles," *Small*, vol. 7, p. 230–234, 2011.